

Article

Motion Characteristics of Collapse Body during the Process of Expanding a Rescue Channel

Yanlong Fu ¹, Kai Xie ¹, Fukun Xiao ^{1,*}, Gang Liu ¹, Zhiyuan Hou ¹ and Rui Zhang ²

¹ Heilongjiang Ground Pressure & Gas Control in Deep Mining Key Lab, Heilongjiang University of Science and Technology, Harbin 150022, China

² Jiamusi Gas Geological Research Limited Company of Longmay Group, Jiamusi 154000, China

* Correspondence: xiaofukun@hotmail.com

Abstract: For the rapid construction of a rescue channel in the process of underground emergency rescue, a method for the expanded rescue channel in the collapse body is proposed and verified by a model test and a numerical simulation experiment. The motion characteristics and motion law of the expanded collapse body are analyzed on the basis of the mechanics of granular media, and a comparative simulation study on the main influencing factors of the collapse body motion is carried out. The results show that: (1) When the collapse body is expanded for a rescue channel, it will form three types of six relative slip planes. According to the position of the slip plane and the distribution of displacement, the collapse body can be divided into a direct displacement region, a stable region, and an indirect displacement region. (2) The expansion process can be divided into the initial start-up stage, the uplift stage, and the collapse stage, according to the formation time of the slip plane and the displacement law of the collapse body. (3) The results of the numerical simulation and the theoretical analysis of the granular media show that the dip angle of the slip plane is determined by the internal friction angle of the collapse particles, and the dip angles of the three slip planes are below $\theta_1 = 90^\circ - \varphi$, $\theta_2 = 45^\circ + \varphi/2$, and $\theta_3 = 90^\circ + \varphi/2$. (4) The transverse scope and longitudinal distance is brought by the expansion increase with the increase in the expansion size, and the simulated dip angles of the slip plane are larger than the theoretical values due to the size effect. (5) In the expansion process, the strong force chain in the collapse body is concentrated in the stress arch above the expander device, and the failure and reconstruction laws of the stress arch at each stage are consistent with the formation of the slip plane and the uplift and instability law of the collapse body.

Keywords: collapse body; emergency rescue; internal friction angle; expansion of the size



Citation: Fu, Y.; Xie, K.; Xiao, F.; Liu, G.; Hou, Z.; Zhang, R. Motion Characteristics of Collapse Body during the Process of Expanding a Rescue Channel. *Appl. Sci.* **2022**, *12*, 11034. <https://doi.org/10.3390/app122111034>

Academic Editor: Ricardo Castedo

Received: 27 September 2022

Accepted: 28 October 2022

Published: 31 October 2022

Publisher's Note: MDPI stays neutral with regard to jurisdictional claims in published maps and institutional affiliations.



Copyright: © 2022 by the authors. Licensee MDPI, Basel, Switzerland. This article is an open access article distributed under the terms and conditions of the Creative Commons Attribution (CC BY) license (<https://creativecommons.org/licenses/by/4.0/>).

1. Introduction

With China's emphasis on coal mine safety production, and the application and promotion of mechanized and intelligent working faces, safe coal mining has been initially realized. However, with the transition of some coal mines from the shallow to the deep mining stage, various disasters are coupled with each other under abominable conditions, such as high gas, high ground stress, and high ground temperature, making post-disaster rescue become more and more difficult. For this reason, emergency rescue is still an important research subject [1]. According to the statistics on coal mine accidents and rescue experiences, the proportion of people killed at the moment of disaster, in the gas (coal dust) explosion, coal and gas outburst, and pressure bumping, is less than 10%, while the deaths of the rest of the people are mostly caused by the lack of oxygen and unavailable supplies and the long period of rescue in the case of the obstruction of the rescue channel [2,3]. Therefore, when the collapse roadway is blocked after the disaster, how to safely and quickly construct a rescue channel in the collapse body for timely rescue has become the key to reducing casualties.

Some domestic scholars have carried out some research on roadway collapse and emergency rescue in collapse bodies. Hao Chuanbo et al. [4,5] classified the collapse types of the mining roadway in the context of a roadway collapse after a dynamic disaster and obtained the relationship between the roadway state and the formation of roadway collapse and blockage by taking the different states of the roadway roof and the two sides as analysis conditions. Shangge Liu et al. [6] studied the unloading behavior of shale under tunnel excavation and drainage conditions through a series of conventional triaxial compression (CTC) tests and unloading confining pressure (UCP) tests and proposed a numerical simulation method of tunnel excavation based on the UCP test. Zhang Guohua et al. [7] analyzed the collapse state of a combined bolt supporting roadway after collapse and predicted the shape of the collapse body. Zhou Xinglong et al. [8] analyzed the collapse state of a collapsed roadway and developed tools such as hydraulic shears, expanders, multi-stage hydraulic props, rescue air cushions, and a high-pressure manual oil pump in order to solve the problems of the cleaning and restoration work of the complex post-disaster roadway and working face that are difficult to complete with the ordinary tunneling and mucking machines. Hao Chuanbo et al. [9,10] proposed to construct a rescue channel by expanding the original roadway, and they carried out force analysis on the reconstructed rectangular channel, achieving very good results. Hongbo Zhao et al. [11] proposed a design optimization method (RBDO) for determining the design parameters of the rock tunnel engineering on the basis of a consideration of the uncertainty and put forward a simple and feasible method for analyzing the uncertainty in rock engineering design, stability analysis, and construction. After the collapse of surrounding rock, the collapse bodies are accumulated and balanced in a discrete state along the original roadway under gravity. At this time, the basic properties and characteristics of the collapse body are consistent with the granular media, and the collapse body can be analyzed and studied with the mechanics of granular media [12].

At present, the theory and the application of granular research, which is similar to that of the collapse body, have been further developed. Han Wenmei [13] analyzed the factors affecting rock frictional sliding and studied the mechanisms affecting rock frictional sliding and the stability from the microscopic level. Sun Hao et al. [14] constructed and simulated near-field ore drawing by physical experiments, numerical simulation, and theoretical analysis and verified the reliability and superiority of discrete element code applied to granular conditions such as caving ore. Cui Wei et al. [15] introduced potential particles into discrete element software, calibrated the parameters of the particle column collapse model based on laboratory tests, and studied the collapse characteristics of the particle column according to the gradation and morphology. Alexander Busch et al. [16] described the rheological properties of particulate matter by means of the two-fluid model combined with the particle flow mechanics theory and closure theory in soil mechanics. With respect to granular simulation, the mechanical behavior and constitutive relationship of particle flow have garnered considerable attention from foreign scholars. Among them, the μ (I) constitutive model and its derived non-local constitutive accurately describe many particle flow phenomena [17–21] and are widely used and developed, but this model still has limitations with regard to particle friction effect and size effect.

With the continuous in-depth research of scholars, the relevant theories and applications of collapse bodies and granular medias have been greatly developed, but the application in emergency rescue is still limited with regard to being an improvement of the old methods. With the fundamental purpose of the rapid construction of a rescue channel in emergency rescue, this paper proposes a method for constructing a rescue channel in the collapse body by means of expansion, and it studies the motion characteristics of collapse bodies in the process of roadway expansion through theoretical analysis, a model test, and a numerical simulation experiment.

2. Expansion Test of Rescue Channel

According to the analysis of Hao Chuanbo et al. [4,7], when disasters such as coal and gas outburst, gas explosion, and fracture zone falling occur, the external force destroys the roadway's surrounding rocks and makes them collapse. A part of the collapsed rocks transforms into granular bodies under the action of the strong external force. After the roadway collapses, the surrounding rocks form a stable elliptical boundary again. Within the boundary, the granular bodies accumulate and block the passage due to the gravity. The expanded rescue channel refers to a rescue channel rapidly constructed in the collapse body by expanding from the bottom along the original roadway. As shown in Figure 1, the green part is the cross-section of the original roadway, the ellipse part is the stable boundary of the surrounding rock, and the red part is the design position of the rescue channel.

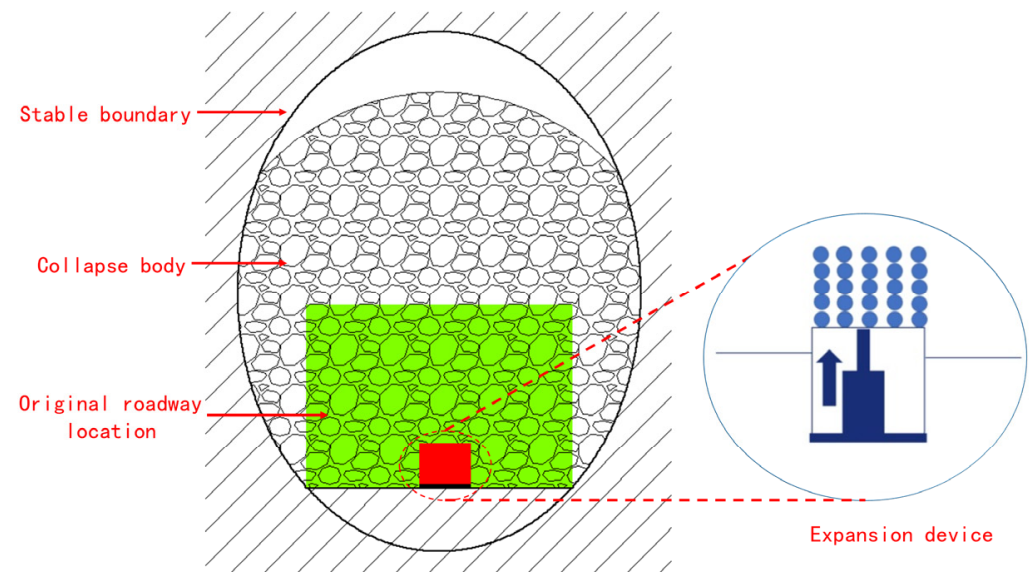


Figure 1. Schematic diagram of rescue channel expansion in collapse body.

2.1. Expansion Test Scheme of Rescue Channel

(1) Design of physical model for expansion test

In the physical experiment, the experimental platform is supported by a similar simulator stand and is completed by building a collapse body, a base plate, an expansion device, and a marked particle. Figure 2 shows that the collapse body has an equal proportion of granular particles made of coal from the roof and floor of the actual roadway and is mixed and arranged according to the particle size proportion of the field investigation and statistics; the base plate is a model constructed by pouring with a strength similar to that of the field floor, which is used to limit the vertical displacement of the collapse body; the expansion device is a jack embedded in the base plate, which can slowly lift the collapse bodies above to simulate the expansion test of the rescue channel (as shown in Figure 3). The marked particles are collapse bodies marked by the color calibration method. They are arranged in layers with a spacing of 0.1 m for the purpose of the overall monitoring of the collapse profile displacement, but they cannot be perfectly arranged in a straight line due to certain differences among the particle sizes. Therefore, by recording and comparing the way of marking the particle positions before and after the expansion test, the law of the collapse body is studied when the rescue channel is constructed by means of expansion.

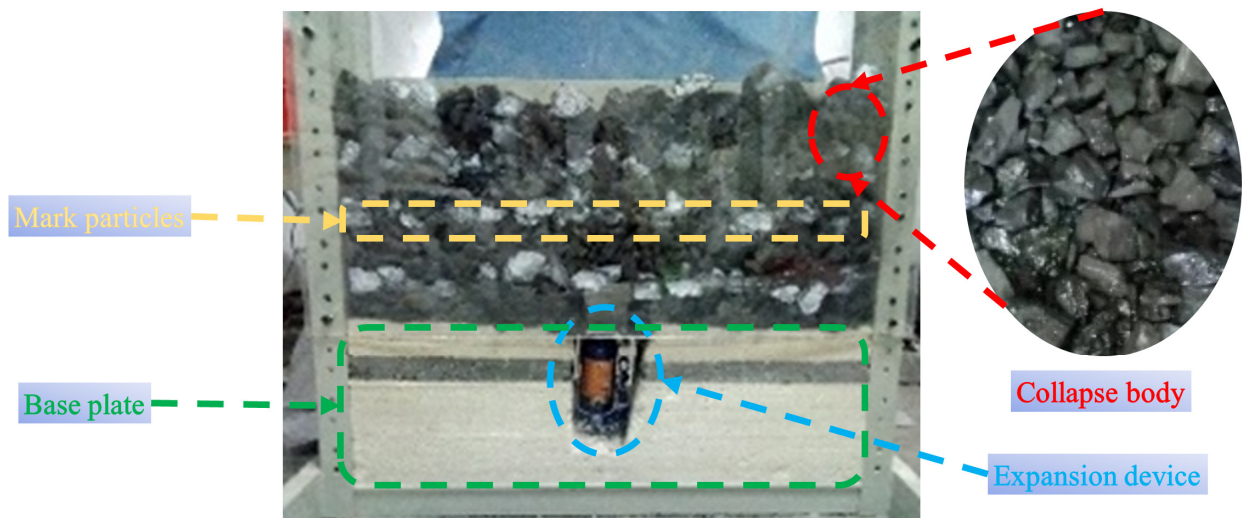


Figure 2. Similar simulation device and collapse body sample.

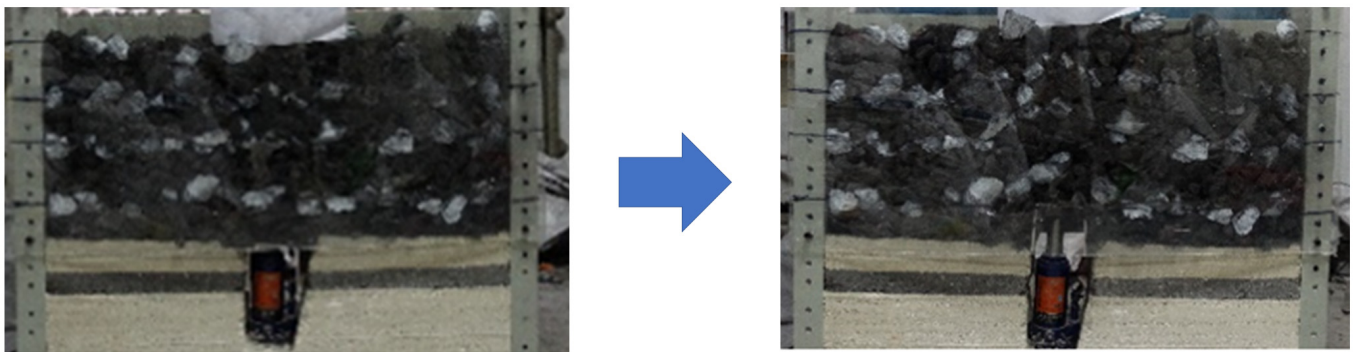


Figure 3. Particle expansion process.

As this test aims to study the motion law of the collapse body, the geometric parameter similarity ratio is taken as the main similarity ratio parameter. The main influencing parameters considered in the simulation device are the width of the expanded channel and the particle size of the collapse body. Therefore, the length similarity ratio of 10:1 and the area similarity ratio of 100:1 are used to meet the requirements of the channel expansion test. In the test, the expansion channel was designed with three different sizes: 0.8 m, 1 m, and 1.2 m. The collapse body can be divided into three particle sizes: 5~10 cm, 10~20 cm, and ≥ 20 cm, with a ratio of 2:2:1, according to the site survey statistics. In addition, since the collapse body materials prepared in the experiment are the same, the comparative test for the materials of the collapse bodies is not designed in the physical experiment. According to the similarity ratio, the specific parameters of the simulation device can be calculated as shown in Table 1.

(2) Design of numerical model for expansion test

With reference to similar simulated tests, the numerical model constructed in PFC (particle flow code) is also composed of the expansion device, the boundary of collapse body, and the collapse body (as shown in Figure 4). The model uses the actual size of $10\text{ m} \times 4\text{ m}$; the expansion device and the boundary of the collapse body are simulated by the wall element, and the collapse body is simulated by the rigid block model; the contact model between the blocks and the block and wall element is a linear parallel bond model. In addition, with reference to the mechanical properties of the actual coal rock, the numerical model parameters of the collapse body (rigid block) and the boundary (wall) of the collapse body are shown in Table 2. For the collapse body shown in Figure 4, the model generates the collapse body by randomly generating irregular shapes based on

the Gaussian function so that there is sufficient internal locking force among the particles of the collapse body. At the same time, the collapse particles are generated according to different particle sizes, and the ratio of the three collapse bodies with different particle sizes is 2:2:1. In order to restore the natural accumulation of collapse bodies, the collapse body is generated at a height of 2 m from the bottom with a relatively sparse density, and it falls and accumulates by gravity. Furthermore, in the simulation, the upper part of the collapse body with enough space is not affected by the roof; so, no overlying load is applied in the model.

Table 1. Similarity ratio calculation.

	Actual Size (cm)	Simulation Experiment Size (cm)	Scale
Width of collapse body accumulation	1000	100	10:1
Height of collapse body accumulation	400	40	10:1
Area of collapse body accumulation	400,000	4000	100:1
Expand the width of channel 1	80	8	10:1
Expand the width of channel 2	100	10	10:1
Expand the width of channel 3	120	12	10:1
Expand the area of channel 1	6400	64	100:1
Expand the area of channel 2	10,000	100	100:1
Expand the area of channel 3	14,400	144	100:1
Particle size 1 of collapse body	5~10	0.5~1	10:1
Particle size 2 of collapse body	10~20	1~2	10:1
Particle size 3 of collapse body	≥20	≥2	10:1

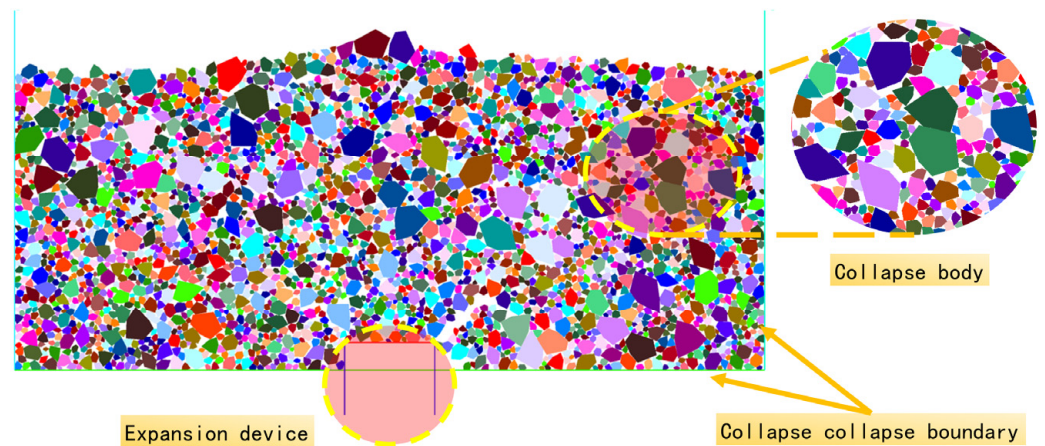


Figure 4. Numerical model of expansion test.

Table 2. Numerical model parameters.

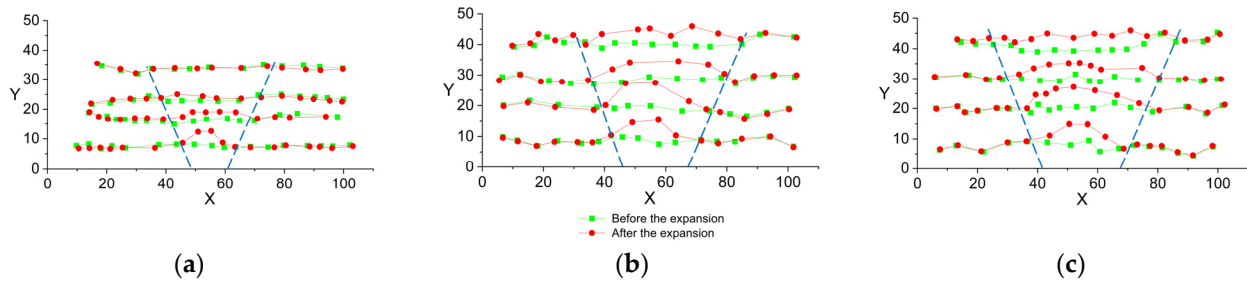
Rigid Block				Wall	
Density (g/cm ³)	Elasticity Modulus GPa	Poisson's Ratio	Friction Coefficient	Elasticity Modulus GPa	Friction Coefficient
1.76	5.81	0.23	0.7536	12	0.7536

2.2. Experimental Phenomena

Figure 5a–c shows the position data of the monitoring points before and after expansion in the physical test, in which the auxiliary line is the boundary between the displacement area and the stable area, and the position change of the monitoring points in the auxiliary line is obviously larger than that outside the auxiliary line. It can be seen by comparing the model positions that the maximum displacement area is mainly concentrated on the collapse particles directly above the expanded channel, and the maximum displacement point is located in the center of the expanded channel, while the monitoring

point outside the auxiliary line has almost no displacement. With the increase in layers, the change of the position before and after the monitoring point corresponding to the position of the expansion device gradually decreases, but the range of displacement gradually expands. With the increase in the size of the expansion device, the displacement of the monitoring point increases continuously, and the position of the monitoring point in the upper layer obviously changes.

Physical experiment:



Numerical simulation:

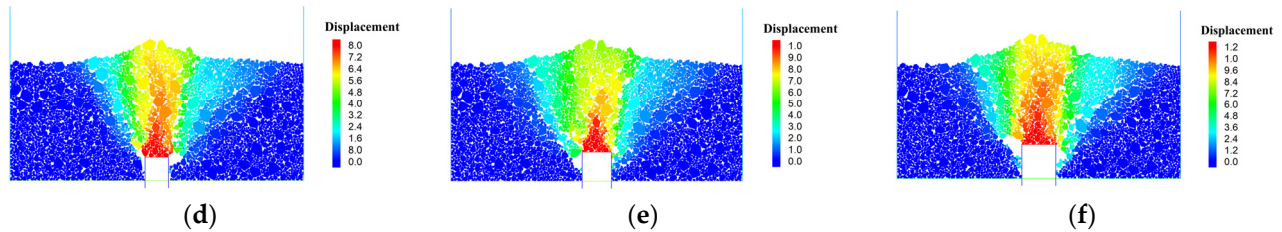


Figure 5. Displacement of collapse body under different expansion sizes: (a) the position of the mark particles when the expansion size is 80 mm; (b) the position of the mark particles when the expansion size is 100 mm; (c) the position of the mark particles when the expansion size is 120 mm; (d) the particles displacement when the expansion size is 0.8 m; (e) the particles displacement when the expansion size is 1.0 m; (f) the particles displacement when the expansion size is 1.2 m.

Figure 5d–f shows the displacement cloud image of the collapse body when the size of the expansion device is 0.8 m, 1.0 m, and 1.2 m, respectively, in the numerical simulation of channel expansion. Compared with the change law of the monitoring point position in the physical test, the two are in good agreement, and the displacement range and displacement size of the collapse body increase with the expansion size. Moreover, the figure also shows that there are obvious divisions in the displacement of the collapse bodies, which is consistent with the data boundary of the physical experimental monitoring points in Figure 5a–c. According to the positional changes of the monitoring points in the physical test and the displacement cloud image in the numerical simulation, the particles can be divided into the following three regions according to the displacement size generated by the collapse particles: the stable region, the direct displacement region, and the indirect displacement region. The stable region is the two approximately right-angled trapezoid regions formed on both sides of the channel after the channel is formed by expansion, and the particles in this region are hardly affected by the expansion process. The direct displacement region is the triangle area directly above the expanded channel, and its displacement size is equal to the height of the expansion device and is triangular in the displacement cloud image. The indirect displacement region is the area where the displacement and position are between the stable region and the direct region. The displacement cloud image shows that each displacement area has a clear boundary with the other displacement regions.

The displacement data and monitoring point data in the numerical simulation and physical test are basically consistent by comparison, and the characteristics of the displacement areas and the boundary of the displacement areas are also almost the same. Therefore,

it is concluded that the numerical model of the expanded test based on the rigid block model and the linear bond contact model is reliable in PFC.

3. Expansion Test Simulation Considering Geometry and Material Properties

In order to further analyze the influence factors of the displacement range and the displacement size of the collapse body and further study the motion characteristics of the collapse body when the rescue channel is constructed by means of expansion, the influence factors of the expanded channel size and internal friction coefficient are compared and analyzed on the basis of the consideration of the actual needs of the expanded rescue channel and the main research contents in the granular research.

3.1. Analysis of the Expansion Process

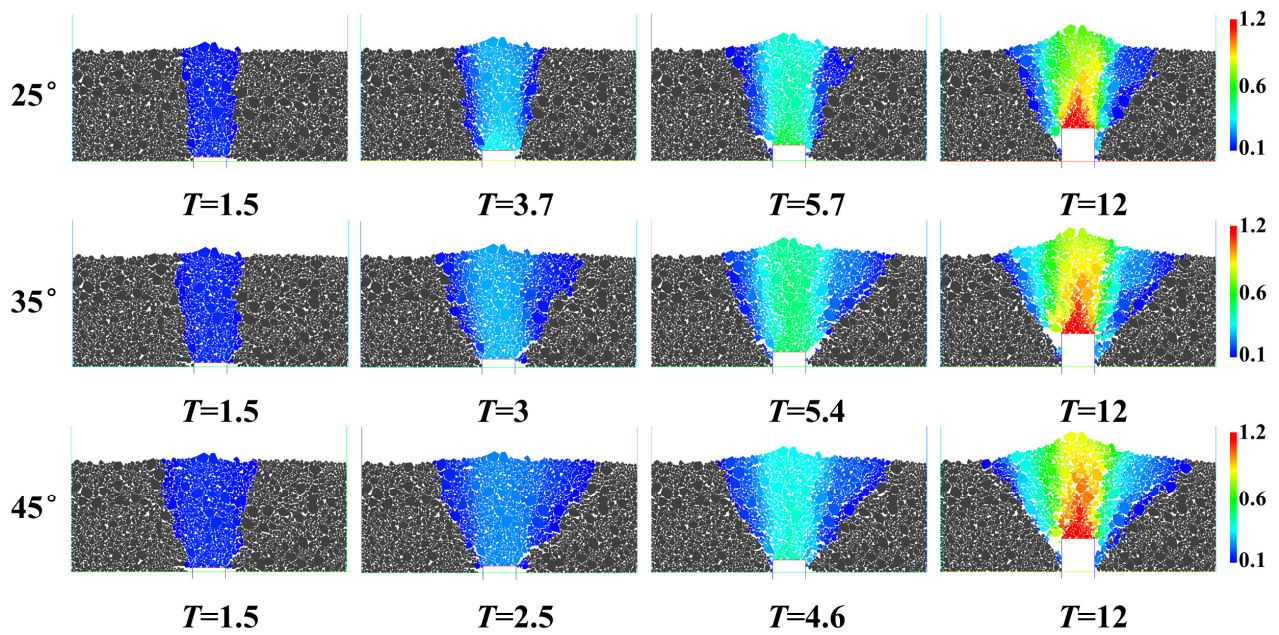
When the rescue channel is expanded in the collapse body at the same lifting speed, there is a deviation in the duration of the different expansion sizes. In addition, different expansion sizes and the properties of the collapse bodies also have a certain influence on the displacement range of the collapse body, but the displacement of the collapse body in the expansion process can still be divided into the same stages. Figure 6 shows the displacement changes of the collapse body in a different time when the size of the expanded channel and the coefficient of internal friction are taken as single variables.

The first stage is the initial start-up stage. The collapse body is lifted during the start-up of the supporting device and is further compacted. At this time, except for the small displacement of the bottom collapse particles directly above the supporting device, the collapse bodies at other positions are in a static or micro-displacement state. With the further uplift of the supporting device, a funnel-shaped displacement region with a small lower part and a large upper part appears in the collapse body, and the displacement region gradually expands with the increase in the displacement, which is embodied in the decrease in the inclination angle of the inclined edge of the funnel-shaped displacement region and the increase in the funnel opening. Furthermore, due to the effect of the interlocking force between the particles of the collapse body, the structure of the particles in the collapse body is relatively stable in the initial start-up stage, and the resistance of the expansion device is relatively large. The first two displacement diagrams of the different expansion tests in Figure 6 show that the duration of this stage is roughly 2.5–3.7 s, corresponding to the expansion height of 0.25–0.37 m, and the expansion process enters the next stage.

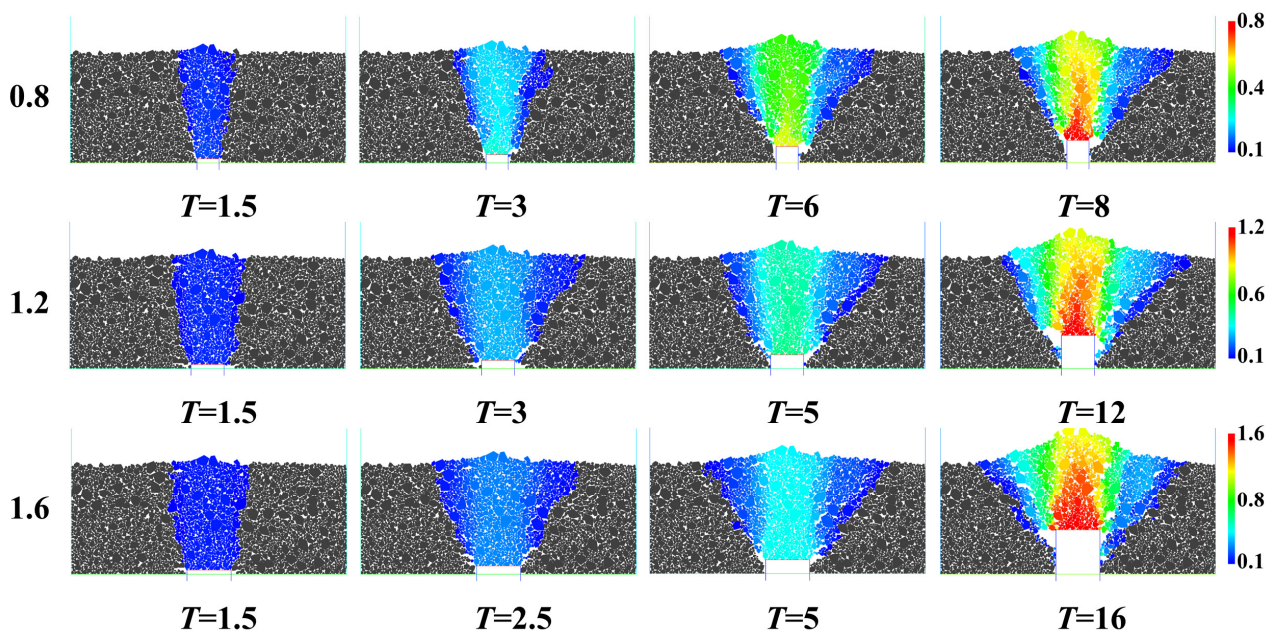
The second stage is the uplift stage; the size of the displacement area of the collapse body is basically determined, and the displacement value in the displacement area continues to increase under the lifting effect of the supporting device. As the collapse body rises, the structure of the collapsed accumulation body becomes loose, as shown by the red boundary in Figure 7b; at this time, the displacement region and the stable region are obviously dislocated along the boundary. As the funnel-shaped displacement region is distributed in a wide position at the top and a narrow position at the bottom, the collapse body is inclined to the displacement region by gravity after rising and is supported by the stable region after redistribution. In addition, the displacement area of the collapse body begins to show obvious direct and indirect displacement divisions at this stage. The duration of this stage is generally still 2.5–3 s; apart from the internal friction angle of 45° , the lifting height of the other working conditions reaches 0.5–0.6 m.

The third stage is the collapse stage. After the funnel-shaped displacement region of the collapse body reaches a certain height, the collapse body in the displacement region will dislocate while the volume increases and will collapse after gradually losing the support of the stable regions on both sides. As shown in the red boundary in Figure 7c, the destabilized collapse bodies begin to slide down to fill the cavities formed by the expanded collapse body. The collapse bodies on the inner side of the boundary still rise with the lifting of the expansion device as a whole, but the collapse bodies above the boundary and the collapse bodies at the bottom also have relative dislocations due to the increase in the

upper volume. This stage lasts the longest, until the expansion device stops lifting, and the relative movement of the particles is also the most complex and frequent in this stage.



(a)



(b)

Figure 6. Displacement change in expansion process under different working conditions: (a) the expansion process of the collapse body with different internal friction angles when the expansion size is 1.2 m; (b) the expansion process of the collapse body with different expansion sizes when the internal friction angle is 37.5°.

increase in the expansion device and the aggravation of the slip in a direct displacement region with the increase in the lifting height.

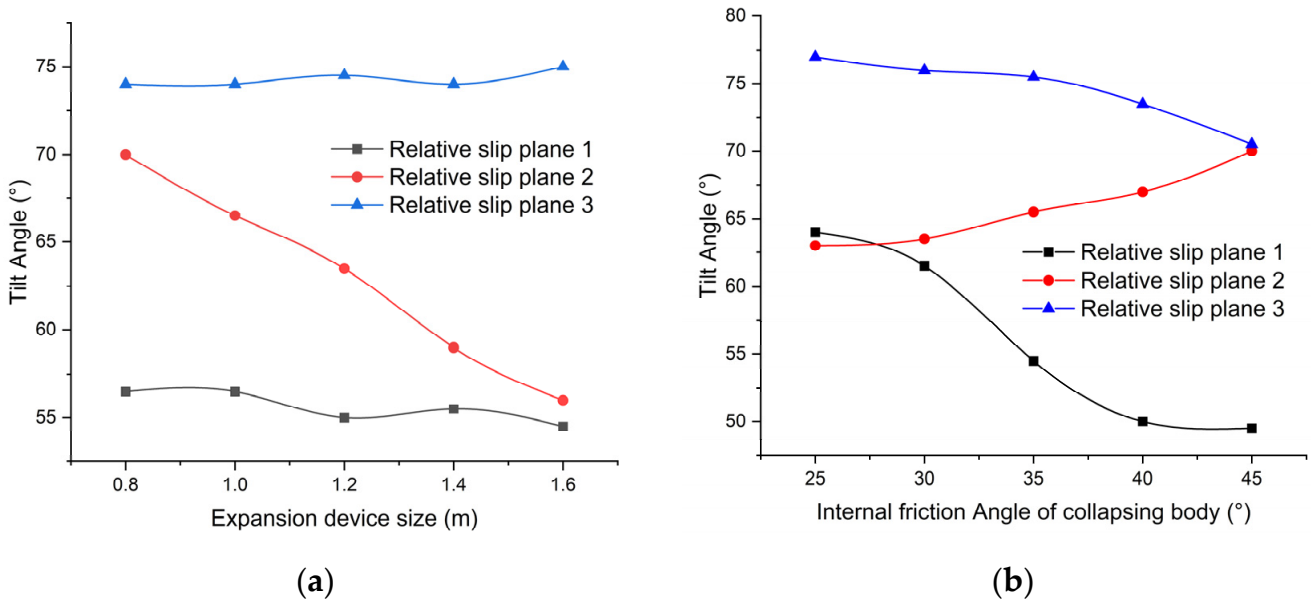


Figure 8. Variation curve of dip angle for the slip plane: (a) the dip angle of the slip plane with different expansion sizes when the internal friction angle is 37.5° ; (b) the dip angle of the slip plane with different internal friction angles when the expansion size is 1.2 m.

Figure 9 shows the variation curve of the maximum width of the displacement region. Obviously, as the internal friction angle and the size of the expansion device in the collapse body increase, the maximum width of the displacement region of the collapse body also increases. When the internal friction angle increases to the maximum, the maximum width of the displacement region is decreased due to the following items: first, it is affected by the boundary conditions of the collapse body. Second, the loose volume caused by the expansion of the collapse body increases with the increase in the internal friction angle.

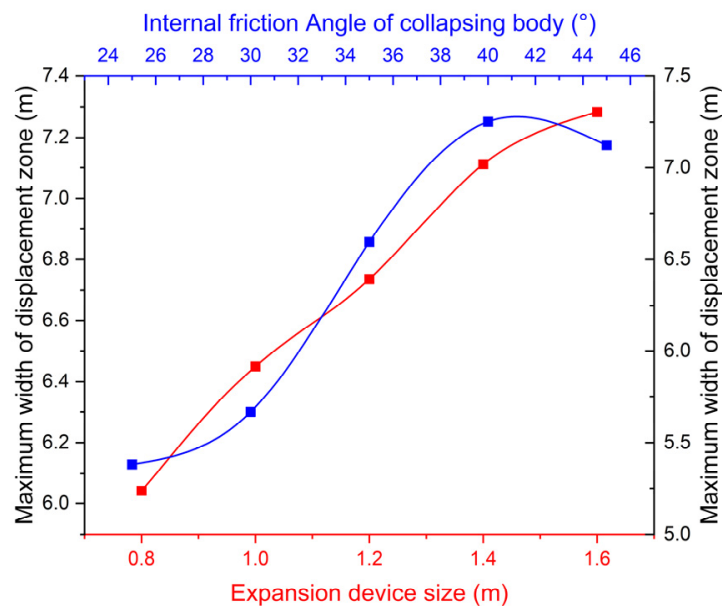


Figure 9. Variation curve of maximum width of displacement region.

4. Analysis of the Movement Mechanism of the Collapse Body in the Expansion Process

4.1. Particle Mechanics Analysis

Unexpanded collapsed accumulation bodies are in a quasi-static state [22], with high solid concentration and relatively stable structure, and their mechanical behavior and structural failure modes are similar to those of solid structures. However, due to the high discreteness of the collapse body, the collapse body above the expansion device will have displacements in different directions and sizes rather than form an overall unidirectional movement [23]. In view of the difference between the quasi-static state and the discrete state before and after the expansion of the collapse body, the mechanical state of the collapse body in the expansion process is analyzed in combination with the relevant theories of solid yielding and granular flow.

When the lower part is expanded, the collapse particles are affected by their own gravity, vertical force, and lateral compressive stress. As shown in Figure 7a, the relative motion of the particles occurs as the expansion device rises, and the collapse body directly above the expansion device is lifted and compacted, while the collapse body at a higher position is loosened, and the horizontal compressive stress in the collapse body gradually decreases with the increase in the porosity between the particles. As shown in the lateral stress curve in Figure 10, when the expansion device is advanced to the position shown in Figure 7b, the relative slip of the collapse body occurs with the increase in the expansion height; the lateral compressive stress of the granular media is the minimum, and the displacement regions are divided into the direct and the indirect displacement regions. Figure 11 shows the stress state of the collapse body at the slip plane in the direct and the indirect displacement regions.

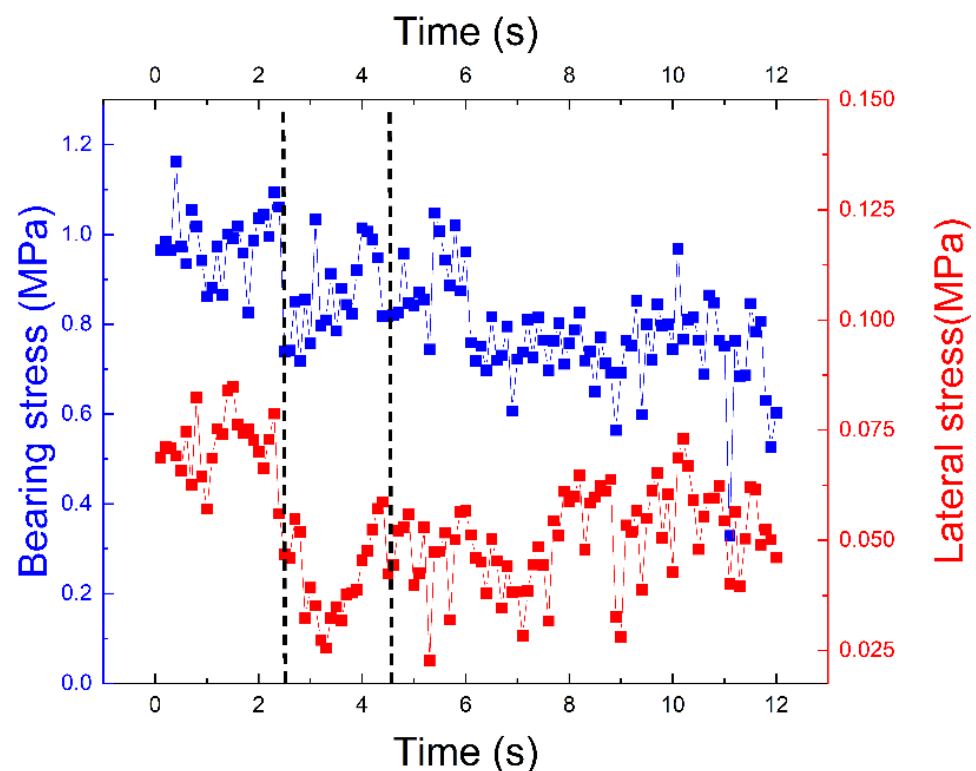


Figure 10. Boundary stress curve.

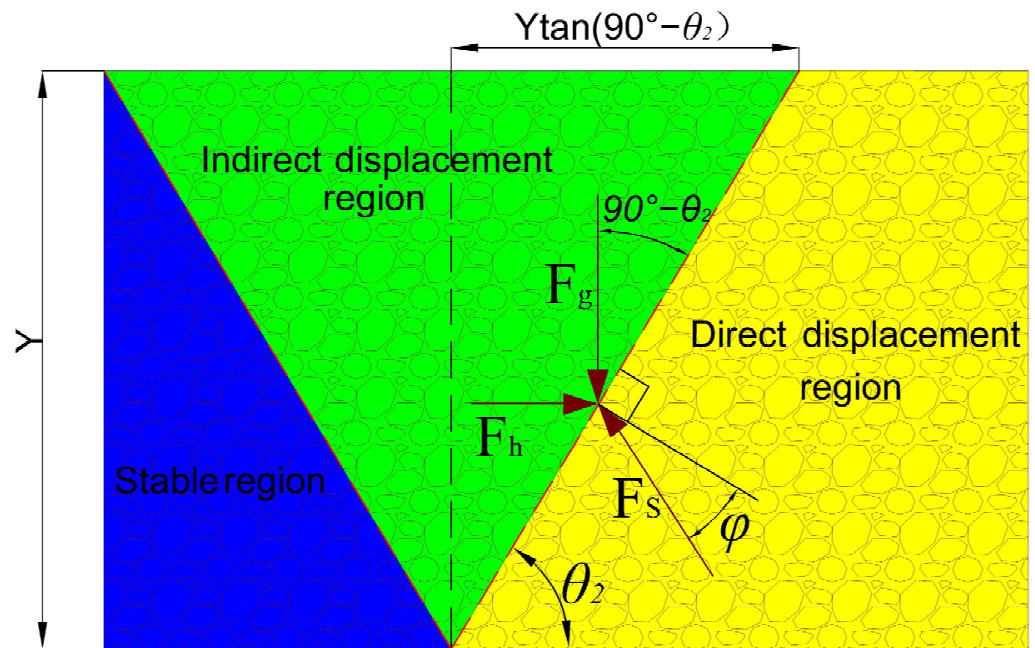


Figure 11. Force analysis of slip plane 2.

At this time, any point on the slip plane is:

$$F_h = F_g \tan(\theta_2 - \varphi) \tag{1}$$

$$F_g = \frac{Y^2 \rho g \tan(90^\circ - \theta_2)}{2} \tag{2}$$

where F_h is the lateral stress value in the collapse body, F_g is the gravity, θ_2 is the dip angle of the slip plane, φ is the internal friction angle of the granular particles, and ρ is the granular particle density.

Let $\tan \varphi = f$, and introducing Equation (2) into Equation (1), we obtain:

$$F_h = \frac{Y^2 \rho g \tan(90^\circ - \theta_2) \tan(\theta_2 - \varphi)}{2} = \frac{Y^2 \rho g (\tan \theta_2 - f)}{2(1 + f \tan \theta_2) \tan \theta_2} \tag{3}$$

$\tan \theta_2$ is always substituted by x ; let $dF_h/dx = 0$ because the lateral stress value F_h of the collapse body at the slip plane is the minimum, and we obtain:

$$\frac{x + fx^2 - (x - f)(1 + 2fx)}{(1 + fx)^2 x^2} = 0 \tag{4}$$

The calculation results are:

$$x = \tan \theta_2 = \tan\left(45^\circ + \frac{\varphi}{2}\right) \tag{5}$$

The dip angle of slip plane 2 is:

$$\theta_2 = 45^\circ + \frac{\varphi}{2} \tag{6}$$

As shown by the red slip plane 1 in Figure 7b, the collapse bodies in the upper indirect displacement region and the lower stable region on both sides of the expansion device also show a relative slip phenomenon with the further expansion of the rescue channel. During the formation of the slip plane, the principal stress leading to the failure of the “solid structure” of the accumulation body is the thrust along the orthogonal direction of

the slip plane 2. Combined with the Mohr–Coulomb failure criterion in the solid structure and the envelope of the accumulation body, the angle between the slip plane 1 and the principal stress is $45^\circ - \varphi/2$. As shown in Figure 12, the dip angle of slip plane is given below according to the geometric derivation

$$\theta_1 = 90^\circ - \varphi \tag{7}$$

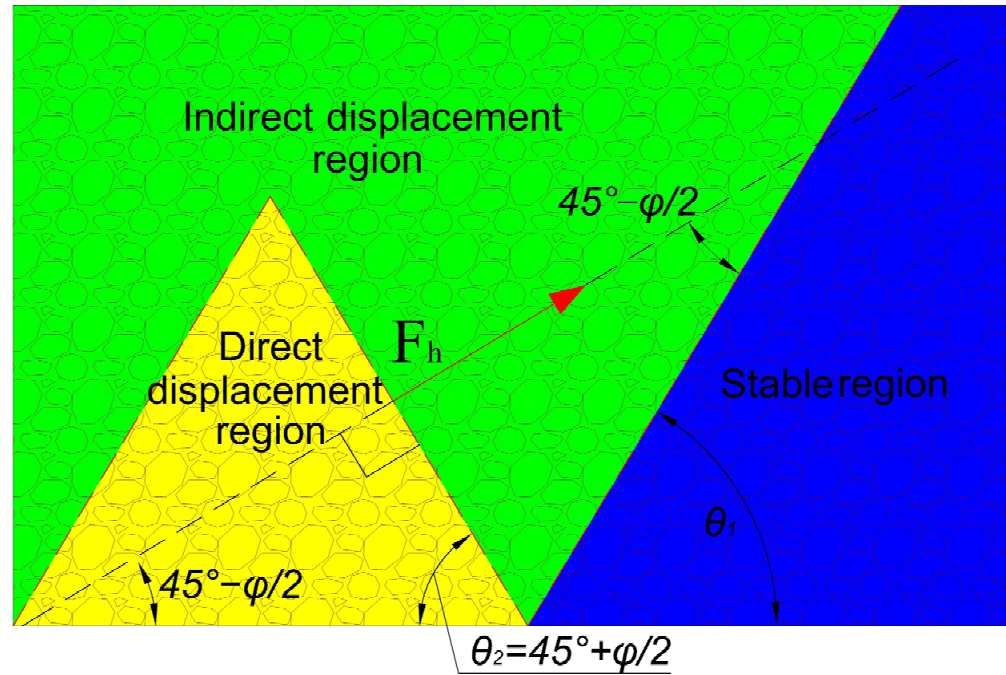


Figure 12. Force analysis of slip plane 1.

As shown in Figure 10, the lateral compressive stress of the granular media falls again with the further expansion of the collapse body; the supporting stress of the expander and the supporting effect of the stable region on the displacement region decrease synchronously, and the friction on the slip plane of the direct and indirect displacement regions increases gradually. As the action direction of the principal stress in the indirect displacement region gradually shifts upward, the included angle of the failure surface in the accumulation body also shifts upward, and a slip plane 3 is formed in the indirect displacement region, as shown in the red line in Figure 7c. It can be inferred by combining the dip angle data of the slip plane 3, measured by numerical simulation, that the inclination of slip plane 3 satisfies:

$$\theta_3 = 90^\circ + \frac{\varphi}{2} \tag{8}$$

The dip angle of the simulated slip plane is slightly larger than the theoretical value given by comparing the dip angle data of the slip plane in Figure 8 and the theoretical value calculated as per Equations (6)–(8). In Figure 8a, the dip angle of slip plane 2 decreases with the increase in the expansion size and gradually approaches the theoretical value. Therefore, it is considered that the size effect has the effect of amplifying the dip angle of the slip plane.

4.2. Particle Contact Evolution Analysis

In the granular accumulation, the contact between particles reflects the characteristics of the solid structure, the stress distribution, and the motion state of the collapse body. Figure 13 is the distribution diagram of the contact force chain in the collapse body at different expansion heights. It shows that when the collapse body expands with the expansion device, the collapse body forms an umbrella-shaped stress arch structure above

the expansion device, and the arc arch of the stress arch structure expands with the increase in the expansion height. In addition, the principal stress in the collapse body on both sides develops directly upward with the rise of the expansion device according to the distribution of the strong force chain in the collapse body.

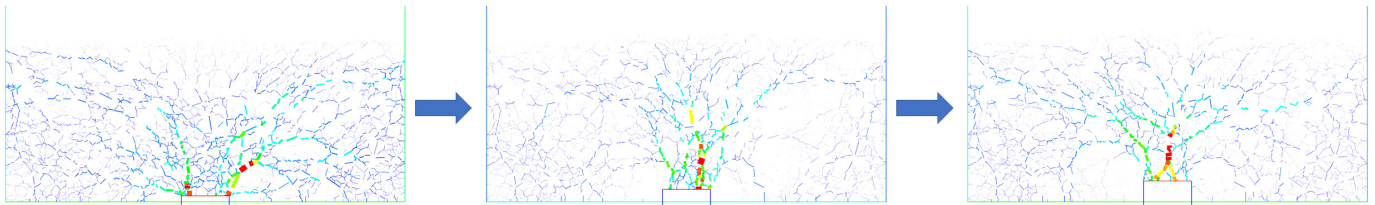


Figure 13. Evolution of force chain grid.

The proportion of the strong force chain and the coordination number of particles are two characterizations of particle contact. The proportion of the strong force chain reflects the stability of the accumulation body, and the coordination number reflects the change in the porosity of the collapse body. Figure 14 is the evolution curve of the proportion of the strong force chain and the particle coordination number in the collapse body with time under different internal friction angles. The dotted line in Figure 14a refers to the formation time of the slip planes 1 and 3 in the collapse body. It can be seen that the proportion of the strong force chain has decreased significantly, which is consistent with the structural instability caused by the formation of the slip plane of the collapse body. In Figure 14b, the coordination number in the dotted line also shows a similar change rule, but the overall change is relatively small, and the coordination number of the collapse body is weakened to a certain extent.

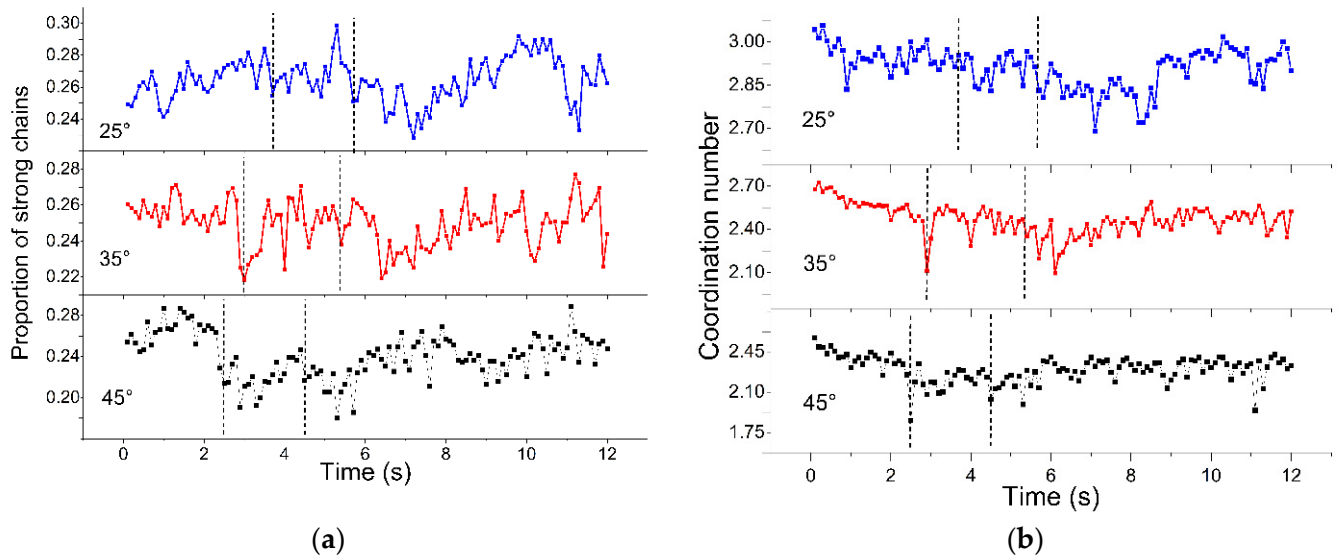


Figure 14. Characteristic evolution curve of contact force chain: (a) the proportion of strong chains at different internal friction angles; (b) the coordination number proportion at different internal friction angles.

When the slip planes 1 and 3 are formed, the dislocation and instability of the displacement region and the stability region exist in the collapse body, leading to the reduction in the contact of the collapse bodies on both sides of the slip plane and the interruption and reconstruction of the strong force chain dominated by the stress arch. The failure of the stress arch causes the collapse body in some displacement regions to slide erratically, as shown in Figure 15; the collapse body converts potential energy into kinetic energy; so, the kinetic energy in the front and rear collapse bodies formed by the slip plane increases to a

certain extent. In addition, it can be seen from the change curve of the potential energy that with the increase in the expansion height, the increase rate of the potential energy of the collapse body increases first and then decreases, which is consistent with the formation and instability of the displacement region in the collapse body.

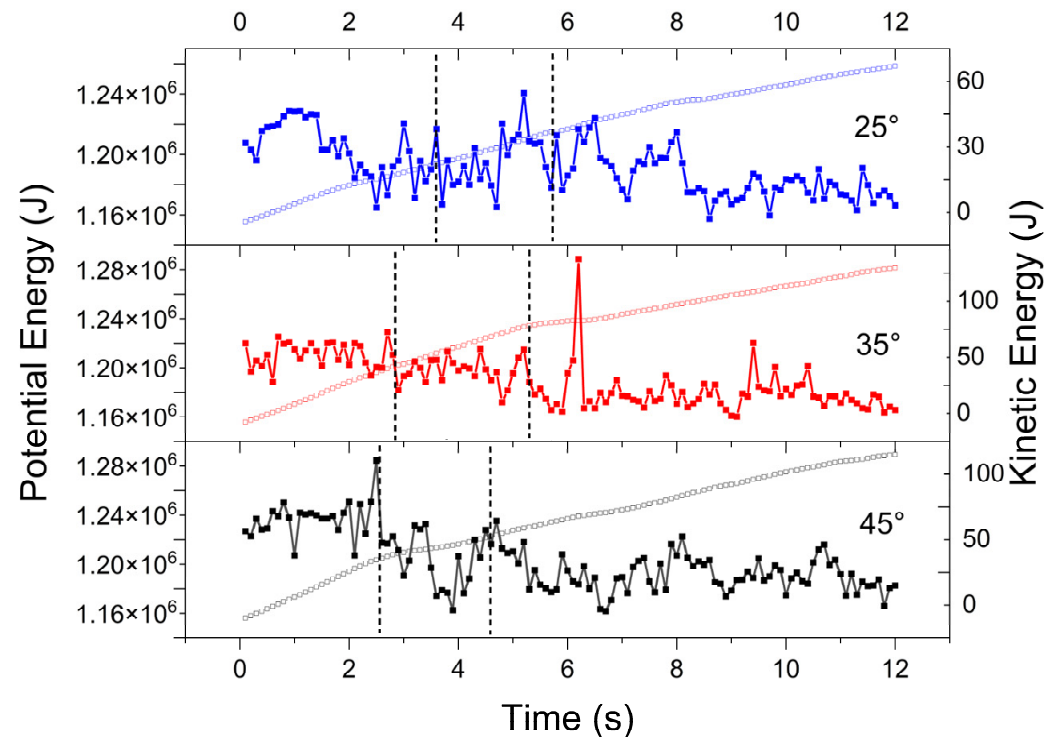


Figure 15. Variation curve of potential energy–kinetic energy.

5. Conclusions

1. The results of the rescue channel expansion test and numerical simulation show that the collapse body will form a slip plane when the expansion device rises. According to the displacement size of the collapse body, the collapse body can be divided into the following: the direct displacement region, the stable region, and the indirect displacement region.
2. A total of six slip planes are formed in the expansion process of the collapse body, and the slip plane can be classified into the following three categories: the boundary between the indirect displacement region and the stable region; the boundary between the direct displacement region and the indirect displacement region; and the instability boundary in the indirect displacement region.
3. The expansion process can be divided into the initial start-up stage, the uplift stage, and the collapse stage according to the formation of the slip plane and the displacement law of the collapse body.
4. Numerical simulation shows that there is a significant correlation between the three slip planes and the size of the internal friction of the collapse particles. Through mechanical analysis and calculation, the dip angles of the three slip planes are $\theta_1 = 90^\circ - \varphi$, $\theta_2 = 45^\circ + \varphi/2$, $\theta_3 = 90^\circ + \varphi/2$.
5. In the expansion process, the strong force chain in the collapse body is concentrated in the stress arch above the expansion device, and the failure and reconstruction laws of the stress arch at each stage are consistent with the formation of the slip plane and the uplift and instability law of the collapse body.

Author Contributions: Conceptualization, F.X.; Data curation, K.X.; Formal analysis, Y.F.; Investigation, Y.F.; Methodology, K.X. and R.Z.; Project administration, F.X.; Supervision, F.X. and G.L.; Writing—original draft, K.X. and F.X.; Writing—review & editing, Y.F., G.L. and Z.H. All authors have read and agreed to the published version of the manuscript.

Funding: The research was funded by the National Natural Science Foundation of China (Grant no. 52074110).

Institutional Review Board Statement: Not applicable.

Informed Consent Statement: Not applicable.

Data Availability Statement: Not applicable.

Conflicts of Interest: The authors declare no conflict of interest.

References

1. Yuan, L. The guest editor of the album “Mine Geological Guarantee under the background of Accurate coal Mining” addressed the readers. *J. China Coal Soc.* **2019**, *44*, 2275–2276.
2. Xiang, G.S. Application of emergency room in mine accident rescue. *Labour Prot.* **2006**, *4*, 92–93.
3. Gao, M.Z.; Sheng, W. Study on Coal Mine Emergency Refuge System Construction in Developed Coal-Producing Countries. *J. Anhui Univ. Sci. Technol. Nat. Sci.* **2011**, *31*, 13–16+67.
4. Hao, C.B.; Zhang, G.H.; Xiao, F.K.; Hu, G. Study of collapse shape about mining gateway under condition of developed joints and fractures roof. *J. Heilongjiang Inst. Sci. Technol.* **2013**, *23*, 1–5.
5. Hao, C.B.; Yu, H.J.; Zhang, G.H.; Pu, W.L. Underground geological fault fracture zone of roadway collapse mechanical properties fall. *J. Heilongjiang Inst. Sci. Technol.* **2016**, *26*, 351–357.
6. Liu, S.G.; Li, Z. Unloading Behaviors of Shale under the Effects of Water Through Experimental and Numerical Approaches. *Int. J. Geomech.* **2022**, *22*, 04022071. [[CrossRef](#)]
7. Zhang, G.H.; Hao, C.B.; Yu, H.J.; Xu, Y.H. Analysis of collapse shape about mining gateway under condition of composite roof after disaster. *J. Heilongjiang Inst. Sci. Technol.* **2014**, *24*, 6–10.
8. Zhou, X.L. Summary of research status of coal mine emergency rescue technology. *Sci. Technol. Inf.* **2007**, *27*, 62.
9. Hao, C.B.; Zhang, G.H.; Hu, G.; Xiao, F.K. Prospect of study on tunnel collapse during rescue following disaster in coal mines. *J. Heilongjiang Inst. Sci. Technol.* **2012**, *22*, 549–552.
10. Hao, C.B.; Zhang, R.; Cheng, Q.L.; Xiao, F.K.; Wang, H.R. Stress analysis of reconstructive rectangular passage in fragmented coal body. *J. Heilongjiang Inst. Sci. Technol.* **2018**, *14*, 114–118.
11. Zhao, H.B. A practical and efficient reliability-based design optimization method for rock tunnel support. *Tunn. Undergr. Space Technol.* **2022**, *127*, 104587. [[CrossRef](#)]
12. Chuanbo, H.; Zhenwen, L.; Fukun, X.; Gang, L.; Rui, Z. The Movement Characteristics of Coal Granular Body in Excavating Rescue Channel in the Collapsed Body. *Adv. Civ. Eng.* **2018**, *6*, 4925828. [[CrossRef](#)]
13. Han, W.M. The Study of Frictional Sliding Characters of Rocks and Its Influencing Factors. Ph.D. Thesis, Taiyuan University of Technology, Taiyuan, China, 2012.
14. Sun, H.; Chen, S.-J.; Gao, Y.-H.; Jin, A.-B.; Qin, X.; Ju, Y.; Yin, Z.-S.; Li, M.-Y.; Zhao, Z.-S. Research on near/far-field flow characteristics of caved ore and rock based on rigid block model. *Chin. J. Eng.* **2021**, *43*, 205–214.
15. Cui, W.; Wei, J.; Wang, C.; Wang, X.H.; Zhang, S.R. Discrete element simulation of collapse characteristics of particle column considering gradation and shape. *Chin. J. Geotech. Eng.* **2021**, *43*, 2230–2239.
16. Alexander, B.; Stein, T.J. Cuttings transport: On the effect of drill pipe rotation and lateral motion on the cuttings bed. *J. Pet. Sci. Eng.* **2020**, *191*, 107136.
17. Lacaze, L.; Kerswell, R.R. Axisymmetric granular collapse: A transient 3D flow test of viscoplasticity. *Phys. Rev. Lett.* **2009**, *102*, 321–324. [[CrossRef](#)] [[PubMed](#)]
18. Andreotti, B.; Forterre, Y.; Pouliquen, O. *Granular Media between Fluid and Solid*; Cambridge University Press: Cambridge, UK, 2013.
19. Zhang, Q.; Kamrin, K. Microscopic description of the granular fluidity field in nonlocal flow modeling. *Phys. Rev. Lett.* **2017**, *118*, 058001. [[CrossRef](#)] [[PubMed](#)]
20. Franci, A.; Cremonesi, M. 3D regularized $\mu(I)$ -rheology for granular flows simulation. *J. Comput. Phys.* **2019**, *378*, 257–277. [[CrossRef](#)]
21. Fei, J.; Jie, Y.; Xiong, H.; Hong, C. A continuum method for granular collapse with $\mu(I)$ -rheology-based dynamic earth pressure coefficient. *Particuology* **2021**, *58*, 214–226. [[CrossRef](#)]
22. Chen, F.Z.; Li, Y.X.; Shi, T.D.; Yan, H. Numerical simulation of full phases of collapse of three-dimensional cylindrical granular pile. *Chin. J. Theor. Appl. Mech.* **2022**, *54*, 1572–1589.
23. Huang, Y.S. *Medium Mechanics*; China Machine Press: Beijing, China, 1993; pp. 3–9.